Journal of Petroleum Science and Engineering 118 (2014) 99–113

Contents lists available at ScienceDirect

Journal of Petroleum Science and Engineering

journal homepage: www.elsevier.com/locate/petrol

Efficient oil displacement near the chamber edge in ES-SAGD

M. Keshavarz, R. Okuno *, T. Babadagli

Department of Civil and Environmental Engineering, School of Petroleum Engineering, University of Alberta, Edmonton, Alberta, Canada T6G 2W2

ARTICLE INFO

Article history:
Received 29 July 2012
Accepted 15 April 2014
Available online 24 April 2014

Keywords:
expanding-solvent–steam assisted gravity drainage (ES-SAGD)
solvent methods
numerical reservoir simulation
thermal oil recovery
phase behavior

ABSTRACT

Steam-assisted gravity drainage (SAGD) is the most widely used method for in-situ bitumen recovery. Expanding-solvent-SAGD (ES-SAGD) has been proposed as an alternative to SAGD to improve its efficiency. In ES-SAGD, steam is coinjected with a small amount of solvent. Detailed oil recovery mechanisms near the chamber edge are little known due to the complex interaction of fluid and energy flow, and phase behavior. Prior research on ES-SAGD explains that coinjected solvent can further decrease oil viscosity near the chamber edge by dilution, in conjunction with heat.

In this paper, we conduct a detailed investigation on oil displacement mechanisms and the placement of solvent near the chamber edge using fine-scale reservoir simulation. The importance of properly considering both phase behavior and flow to design ES-SAGD is demonstrated. Results show that ES-SAGD can achieve a higher displacement efficiency than SAGD. Oil production rate in ES-SAGD can be two times higher than that in SAGD. As a result, the ultimate oil recovery of ES-SAGD is enhanced by almost 20%, compared to SAGD in this research. The oil saturation reduction results from condensed solvent bank and phase transition near the chamber edge. The condensed solvent bank lowers the oil-component concentrations there. The diluted oil with solvent is then redistributed in the gaseous and oleic phases in the presence of the water phase on the phase transition at the chamber edge. The resulting amount of the oleic phase can be significantly small, yielding lowered oil saturations in the ES-SAGD chamber.

1. Introduction

Efficient recovery of unconventional oil resources, such as heavy oil and bitumen, is becoming more important considering the ever increasing energy demands. The main challenge in in-situ recovery of bitumen is its extremely high viscosity, which makes it essentially immobile at initial reservoir conditions. The most widely used method for bitumen recovery is steam-assisted gravity drainage (SAGD) (Butler, 1997). SAGD takes advantage of the strong temperature dependency of bitumen viscosity. Viscosity of a typical bitumen falls several orders of magnitude over the temperature range of 10–200 °C. In SAGD, steam of a high quality is injected using a horizontal injection well, which is located a few meters above a horizontal production well. Bitumen is mobilized by the latent heat released by the steam injected. Gravity is the main driving force for the mobilized oil to drain towards the production well. The disadvantages of SAGD are the costs and CO_2 emissions associated with generation of a significant amount of steam.

Expanding-solvent–steam assisted gravity drainage (ES-SAGD) has been proposed as an alternative to improve the efficiency of SAGD. In ES-SAGD, a small amount of hydrocarbon solvent is coinjected with steam to further reduce the viscosity of bitumen near the chamber edge (Nasr and Isaacs, 2001; Nasr et al., 2003). Gates (2007) reported that ES-SAGD requires a smaller amount of steam to recover the same amount of bitumen, compared to SAGD.

ES-SAGD, if designed properly, also can exhibit higher oil production rate than SAGD (Nasr et al., 2003; Gates, 2007; Ivory et al., 2008; Li and Mamora, 2010; Li et al., 2011a, 2011b; Yazdani et al., 2011). These studies cover a wide range of solvents (such as pure hydrocarbons from C_5 through C_8 and diluents) and reservoir oils (heavy oil and bitumen). As described in Keshavarz et al. (2013a), the extent of oil rate improvement can vary depending on the reservoir/operating conditions. There is still an ongoing debate on an optimum selection of solvent compounds, solvent concentrations, and operating conditions.

Gates (2007) conducted a simulation study on ES-SAGD with C_6 for the Athabasca bitumen and stated that temperature near the

* Correspondence to: Department of Civil and Environmental Engineering, School of Petroleum Engineering, University of Alberta, 3-114 Markin/CNRL Natural Resources Engineering Facility, Edmonton, Alberta, Canada T6G 2W2.
Tel.: +1 780 492 6121; fax: +1 780 492 0249.
E-mail address: rokuno@ualberta.ca (R. Okuno).

http://dx.doi.org/10.1016/j.petrol.2014.04.007
0920-4105/

Nomenclature

Roman symbols

C_1	methane
C_2	ethane
C_3	propane
C_4	n-butane
C_5	n-pentane
C_6	n-hexane
C_7	n-heptane
C_8	n-octane
C_9	n-nonane
C_{10}	n-decane
C_D	dead-oil component given in Table 2
i	component index
j	phase index
j_o	oil-component molar flux in the oleic phase
k	permeability
k_r	relative permeability
L	oleic phase
u	velocity
V	gaseous phase
W	aqueous phase
x	mole fraction

Greek letters

μ	viscosity
ρ	molar density

Abbreviations

ARC	Alberta Research Council
GCOS	Great Canadian oil sands
LASER	liquid addition to steam for enhanced recovery
SAGD	steam-assisted gravity drainage
ES-SAGD	expanding-solvent–steam assisted gravity drainage
IFT	interfacial tension
VAPEX	vapor extraction

chamber edge in ES-SAGD can be lower than that in SAGD due to gaseous solvents accumulated there. Vapor–liquid phase behavior of solvent–steam systems resulting in such temperature profiles was given in Dong (2012) and Keshavarz et al. (2013a, 2013b) in detail. Higher production rates during ES-SAGD can be achieved only if the dilution effects of the coinjected solvent can offset the temperature reduction effect on the oleic (L) phase viscosity near the chamber edge. This indicates that understanding of the mechanisms in ES-SAGD requires detailed investigation of the non-isothermal multiphase flow near the chamber edge.

A few papers on steam–solvent coinjection indicated that it can reduce oil saturation below a residual oil saturation obtained from SAGD. Nasr and Ayodele (2006) observed that residual oil saturations in their ES-SAGD experiments were lower than those in SAGD. They used a Cold-Lake-type live oil and a C_4–C_{10} mixture as the coinjected solvent. Deng et al. (2010) conducted ES-SAGD experiments with the Athabasca bitumen and a diluent coinjected with steam. They presented figures indicating reduced oil saturations inside the ES-SAGD chamber, but their details were not discussed. Li et al. (2011a) conducted solvent-aided-SAGD experiments with the Athabasca bitumen and two different solvents: C_7 and a mixture of C_7 and xylene. They stated that theoretically, liquid solvent can flush out all residual oil. However, they did not explain how such miscibility can be developed in steam–solvent coinjection for bitumen. Yazdani et al. (2011) investigated numerical simulations of coinjection of n-alkanes ranging from C_3 to C_7 with steam for the Athabasca bitumen. They stated that lowered oil saturation could be attributed to the interfacial tension (IFT) reduction between phases during steam–solvent coinjection and the solvent amount in the residual oil phase. They recommended modifying the end-point saturations of relative permeability curves according to laboratory tests to capture IFT reduction in the dynamic coinjection simulation. Jha et al. (2013) explained the reduced residual oil saturation as a result of the partial evaporation of the condensed solvent that was mixed with bitumen. They reported that the residual oil saturation at a given point in the reservoir was correlated to the historic peak of the solvent concentration at that location. However, detailed mechanisms for the enhanced local displacement efficiency were not presented in their paper.

There are also field observations of improved production rates by coinjection of solvent with steam. In EnCana's Solvent Aided Process (SAP) in 2002 at Senlac, oil rate was improved by 50% shortly after butane was coinjected with steam in phase-C well pairs, which had been operated under SAGD. Similar improvement was reported after applying SAP in their Christina Lake project (Gupta et al., 2005; Gupta and Gittins, 2006). In another application of solvent–steam coinjection by Imperial Oil in Cold Lake, diluent was coinjected with steam in selected wells in their last cycles of cyclic steam stimulation (CSS). This application of coinjection was called Liquid Addition to Steam for Enhanced Recovery (LASER) and resulted in about 100% incremental oil production rates (Leaute, 2002; Leaute and Carey, 2005).

Interpretation of field pilots for this non-isothermal solvent process can be complicated by the complexities that exist in bitumen reservoirs. The heterogeneities of Athabasca bitumen reservoirs were described in Redford and Luhning (1999). As reported in the literature extensively, the local geology and petrophysics played a major role in SAGD operations (Edmunds et al., 1989; Redford and Luhning, 1999; Kisman and Yeung, 1995; Le Ravalec et al., 2009).

Edmunds et al. (1989) stated that low vertical permeability can damage the vertical rise of the chamber. As a result, the neighboring chambers may coalesce before reaching the top of the reservoir, leaving greater residual oil saturations in the top portion of the reservoir. Hosseininejad Mohebati et al. (2010) speculated that the vertical permeability can affect the heat transfer to the bitumen and the overburden when a gas layer forms near the chamber boundaries during the coinjection of non-condensable gases.

The generally isotropic McMurray oil sands are randomly interspersed with irregular shale bodies (Edmunds et al., 1989). The impact of shale barriers depends on their locations relative to well pairs. Barriers located between the injector and producer can inhibit the local steam-chamber development, even when they are small and discontinuous. For such a case, fractions of the well-pair horizontal section do not effectively contribute to the production for a long period (Le Ravalec et al., 2009). The effect of small and discontinuous barriers in other locations of the reservoir is likely less severe. They can be bypassed by the steam. Also, they can increase the contact area between the steam chamber and bitumen. A continuous barrier with only a few breaks may still allow for steam transport through these breaks; however, it can severely restrict the drainage of the L phase (Edmunds et al., 1989).

The effects of heterogeneities on SAGD and vapor extraction (VAPEX) were also discussed by Jiang and Butler (1996) in their experimental research.

The effects of heterogeneities on the performance of solvent–steam coinjection processes are relatively unknown in the literature. Results of Hosseininejad Mohebati et al. (2010) indicate that petrophysical properties of the reservoir can change the economic feasibility of coinjection of non-condensable gases with steam. Suranto et al. (2013) conducted a simulation study of steam–solvent coinjection using a three-dimensional (3-D) heterogeneous reservoir model. Their results indicate that optimization of steam/solvent distribution can be further complicated by the varying temperature and pressure along the well-pair horizontal section.

As described in Keshavarz et al. (2013a), a number of proposals for optimal solvent–steam coinjection presented in the literature were based on simplified reservoir and phase behavior models, such as a vertical 2-D reservoir with a homogeneous permeability/porosity field, a K-value-based fluid model with only a few components, no asphaltene precipitation, no capillary, and no physical dispersion.

The main objective of the current paper is to clarify how ES-SAGD can achieve higher oil production rate and displacement efficiency than SAGD. A series of fine-scale simulations are conducted using a vertical 2-D homogeneous reservoir model. This simplification of the reservoir model allows us to focus on the detailed mechanistic study near the chamber edge resulting from the 2-D propagation of heat and components in the reservoir.

We first describe simulation cases performed in this research. Results of numerical simulations are then explained in terms of oil production rate and displacement efficiency in ES-SAGD and SAGD. It is shown that ES-SAGD can achieve high displacement efficiency without considering IFT reduction in simulation. Phase equilibrium in temperature and composition space near the chamber edge plays important roles in the oil displacement mechanism.

2. Description of simulation cases

Simulations are conducted using the STARS simulator of Computer Modeling Group (2011). The 2-D reservoir model used in this research consists of 70, 1, and 20 gridblocks in the *x*, *y*, and *z* directions, respectively. A uniform gridblock size of $1.0 \times 37.5 \times 1.0\ m^3$ is used, which results in model dimensions of 70.0 m, 37.5 m, and 20.0 m in the *x*, *y*, and *z* directions, respectively. The injection well is located 4.0 m above the production well, which is located 3.0 m above the bottom of the reservoir model. The simulations are performed only for a half of the SAGD/ES-SAGD chamber. Thus, the wells are placed in the left-most grids of the 2-D reservoir model.

The initial reservoir pressure and temperature are 1500 kPa and 13 °C, respectively. The initial oil saturation is 0.75. The aqueous (W) phase initially exists at its irreducible saturation of 0.25. Key properties of the homogeneous reservoir are given in Table 1. The temperature-independent relative permeabilities used are shown in Fig. 1. The temperature dependency of relative permeabilities is not considered in this research. It is difficult to predict the effects of increased temperature on relative permeabilities. As mentioned in Polikar et al. (1990), results of carefully conducted experiments showed that the temperature effects were system specific. Frequently observed effects presented by Nakornthab and Evans (1986) include an increase in irreducible water saturation, a decrease in residual oil saturation, an increase in relative permeability to oil, and a decrease in that to water. This may be related to the presence of clays and minerals in the rock, as well as wettability and contact angle changes with an increase in temperature (Farouq Ali, 2007). However, significant temperature effects were not reported during the experiments conducted by Polikar et al. (1990) for the Athabasca bitumen/water system in clean or reservoir sands.

Capillarity, hysteresis, and asphaltene precipitation are also not considered in this research. There are several reports of asphaltene precipitation during recovery processes involving solvents in the

Table 1
Reservoir rock and fluid properties used in the simulation cases.

Properties	Values
Porosity	33%
Horizontal permeability	4000 md
Vertical permeability	3000 md
Initial reservoir pressure at depth of 500 m	1500 kPa
Initial reservoir temperature	13 °C
Initial oil saturation	0.75
Initial water saturation	0.25
Three-phase relative permeability model (CMG, 2011)	Stone's model II
Formation compressibility	1.8E−5 1/kPa
Rock heat capacity (Butler, 1997)	2600 kJ/m^3 °C
Rock thermal conductivity (Butler, 1997)	660 kJ/m day °C
Over/underburden heat capacity (Butler, 1997)	2600 kJ/m^3 °C
Over/underburden thermal conductivity (Butler, 1997)	660 kJ/m day °C
Bitumen thermal conductivity (Butler, 1997)	11.5 kJ/m day °C
Gas thermal conductivity (Yazdani et al., 2011)	2.89 kJ/m day °C
Water thermal conductivity	1500 kJ/m day °C

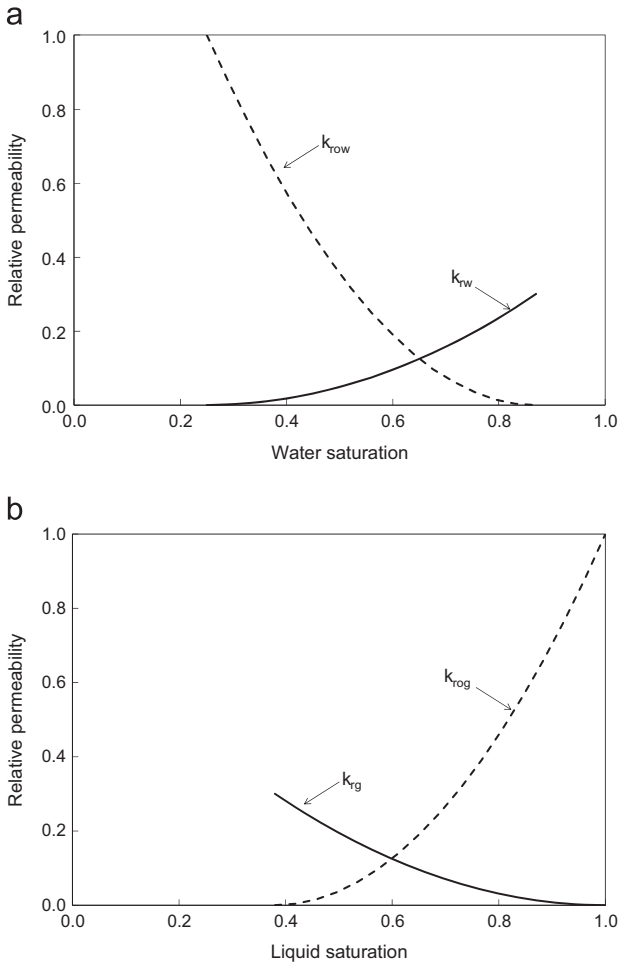

Fig. 1. Relative permeability curves used in the simulation cases; (a) the water–oil system and (b) the oil–gas system.

literature (Leontaritis and Mansoori, 1987; Mokrys and Butler, 1993; Das and Butler, 1998; Nghiem et al., 2001; Akbarzadeh et al., 2004; Haghighat and Maini, 2008; Mohammadzadeh et al., 2010). Asphaltene deposition around the well bore, well tubings, flow lines, and other equipment has threatened the economic recovery of oil in many occasions (Leontaritis and Mansoori, 1987). In-situ de-asphalting can be advantageous since it reduces the oil viscosity and leads to production of upgraded oil as reported by Mokrys and Butler (1993) and Haghighat and Maini (2008). Gupta and Gittins (2006) also reported an improvement in the API gravity of the produced oil from EnCana's SAP pilot in Senlac, in which butane was coinjected with steam. Precipitation of asphaltene even improved the production rate due to in-situ upgrading and viscosity reduction in Das and Butler (1998).

Badamchizadeh and Kohse (2011) developed an equation-of-state (EOS) model for the asphaltene precipitation during ES-SAGD with heptane. They used CMG-WinProp Asph/Wax multi-phase flash calculation and simulated the process with STARS thermal simulator. Their technique was to split the heaviest pseudo-component of their reservoir oil into two pseudo-components, a non-precipitating and a precipitating fraction in order to obtain a quantitative match with experimental data. The parameters that need to be adjusted were binary interaction coefficients between the precipitating component and lighter components, the solid-phase molar volume, the solid–liquid heat capacity difference, the heat of fusion at the triple point, and the triple point temperature of the precipitating component. Solid–liquid *K*-values were then generated from flash calculations for non-equilibrium reaction. However, experimental data for n-alkane and bitumen mixtures are scarce in the literature. Particularly, the solid phase precipitation should be studied at different pressure, temperature, and mole fractions of solvent (Badamchizadeh and Kohse, 2011). Simulations of Badamchizadeh and Kohse (2011) showed that asphaltene precipitation would not have a significant impact on the steam-chamber growth if the blockage effect was small.

For the Athabasca (GCOS) bitumen, a four-pseudo-component characterization was developed by Johnson (1985) and was further investigated by Mehrotra and Svrcek (1987). The bitumen model based on pseudo-components was shown to give satisfactory estimations of vapor–liquid equilibrium (Sarkar, 1984). Based on this four-pseudo-component model, properties of bitumen as a single pseudo-component were also presented by Mehrotra and Svrcek (1987). These properties are presented in Table 2 and are used throughout this work. Reducing the number of pseudo-components may cause deviation of the phase behavior model from that of a real bitumen–solvent mixture. However, it is adequate for the purpose of the current mechanistic study. It allows us to identify clearly the responsible mechanisms for improved oil production rates and/or displacement efficiency associated with ES-SAGD. Also, schematic illustration of recovery mechanisms is possible on simple ternary diagrams as will be shown later.

Viscosity of gas-free Athabasca (ARC) bitumen is estimated as a function of temperature using the correlation proposed by Mehrotra and Svrcek (1986) and is presented in Fig. 2. The pressure dependency of bitumen viscosity is neglected in this study. A typical gas–oil ratio (GOR) for Athabasca oil sand is about 2.0 m^3/m^3 (Ivory et al., 2008). We make a live oil using a GOR of 1.8 m^3/m^3, methane (C_1) for the gas, and the dead-oil component (C_D) given in Table 2. The resulting mole fraction of C_1 in the live oil is 0.04. Fig. 3 shows the vapor pressure curves of C_1 and C_D, and the critical locus of the live oil. The critical locus of the live oil at high C_1 concentrations cannot be found using the Peng–Robinson (PR) EOS (Peng and Robinson, 1976) within the pressure range shown.

Table 2
Properties of the dead-oil component (C_D).

Properties	Values
Molecular weight	594.6 kg/kg mole
Critical pressure	785.98 kPa
Critical temperature	817.75 °C
Acentric factor	1.361
Normal boiling point	663.95 °C
Specific gravity	1.077

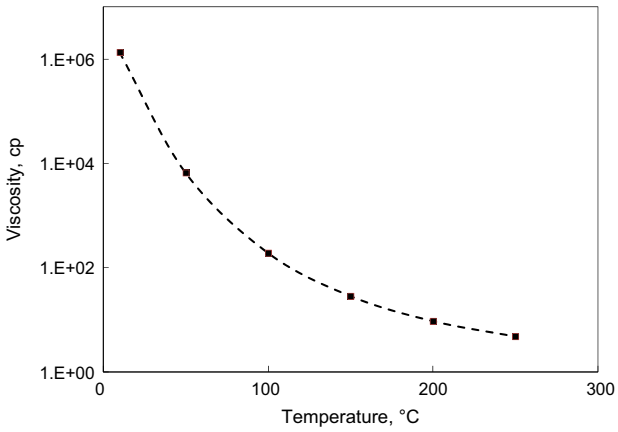

Fig. 2. Viscosity of bitumen (the C_D component in Table 2) at different temperatures.

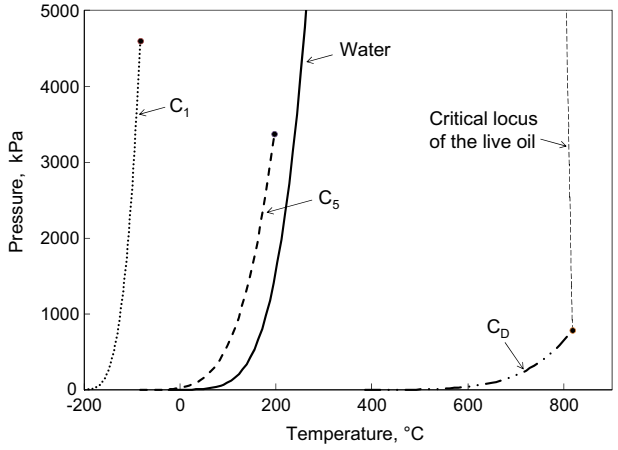

Fig. 3. Vapor pressure curves of C_1, C_5, C_D, and water, and the critical locus of the live oil (a mixture of C_1 4% and C_D 96%). The critical locus of the live oil at high C_1 concentrations cannot be found using the PR EOS within the pressure range shown. The black circles indicate the critical points of the hydrocarbon components.

The injection and production wells are operated at constant bottom-hole pressures of 2730 kPa (maximum) and 1500 kPa (minimum), respectively. The steam table indicates that the saturated steam temperature at 2730 kPa is 228.7 °C. A maximum flow rate of 1.0 m^3/day is assigned to steam at the production well to control steam production during the simulation. Preheating of the reservoir is performed for 6 months.

A steam quality of 0.9 is used in all simulations. As a solvent, n-pentane (C_5) is coinjected with steam at 2.0 mol%. The key properties of C_5 are listed in Table 3. Binary interaction parameters are 0.0206 for C_1–C_5, 0.1174 for C_1–C_D, and 0.04453 for C_5–C_D. Fig. 3 shows the vapor pressures of water and C_5. The condensation temperature of C_5 at the injection pressure, 2730 kPa, is lower than that of water.

There are four components in the simulations: water, C_1, C_5, and C_D. The STARS simulator represents the fluid phase behavior using *K*-value tables. Constant-*K* flash with the Rachford–Rice

Table 3
Properties of n-pentane (C_5).

Properties	Values
Molecular weight	72.1 kg/kg mole
Critical pressure	3374.12 kPa
Critical temperature	196.45 °C
Acentric factor	0.251
Normal boiling point	36.05 °C

equations (Rachford and Rice, 1952) is used to calculate up to three equilibrium phases (L, gaseous (V), and W). The *K*-values for the hydrocarbon components, C_1, C_5, and C_D, are generated by performing a series of flash calculations using the PR EOS with the van der Waals mixing rules. Composition dependency of *K*-values is not considered within an individual simulation in this research. A mixture of 20% C_5 and 80% live oil, which consists of 96% C_D and 4% C_1, is used for generating *K*-values for the hydrocarbon components.

Hydrocarbon *K*-values can be also generated internally in the STARS simulator using a correlation. However, such a correlation should be carefully used for ES-SAGD simulation because *K*-values can significantly affect solvent propagation in the simulation. More reliable *K*-values can be generated using an EOS as in this research. Also, more detailed compositional phase behavior can be modeled in simulation if a plus fraction of the reservoir oil is modeled using a reliable heavy-oil characterization method (e.g., Kumar and Okuno, 2013) and PVT data available.

The *K*-values for the water component at a given temperature are assumed to be the saturation pressure of water at that temperature divided by the total pressure. It is also assumed that the W phase consists of only the water component, and the L phase consists of only hydrocarbon components. The water and hydrocarbon components can coexist in the V phase.

The mixing rule used for viscosity of phase j, μ_j, is

$$\ln(\mu_j) = \sum_{i=1}^{N_C} x_{ij} \ln(\mu_{ij}), \quad (1)$$

where N_C is the number of components, x_{ij} is the mole fraction of component i in phase j, and μ_{ij} is the component viscosity of component i in phase j. The mixing rule used for molar density of phase j, ρ_j, is

$$\frac{1}{\rho_j} = \sum_{i=1}^{N_C} \frac{x_{ij}}{\rho_{ij}}, \quad (2)$$

where ρ_{ij} is the component molar density of component i in phase j.

Fig. 4 shows the oil recovery histories for the ES-SAGD and SAGD simulations, where the amount of solvent recovered is not considered for the ES-SAGD plots. There are two main differences between the two recoveries. One is the higher oil production rate observed for ES-SAGD, and the other is the ultimate oil recovery enhanced by ES-SAGD. These two points will be discussed in Sections 4 and 5. We show that efficient ES-SAGD involves accumulation of solvent near the chamber edge, which will be discussed in the subsequent section.

As mentioned earlier, a mixing ratio of C_5 with the live oil is set to 0.2 when generating *K*-values for the simulation. Another mixing ratio of 0.6 is tested to observe the potential effects on ES-SAGD simulation results. Fig. 4 compares oil recoveries for the two mixing ratios. The effect of the mixing ratio used on oil recovery prediction is not significant in this case. The slight difference observed is due to different phase compositions predicted during the simulations. Simulations were also conducted

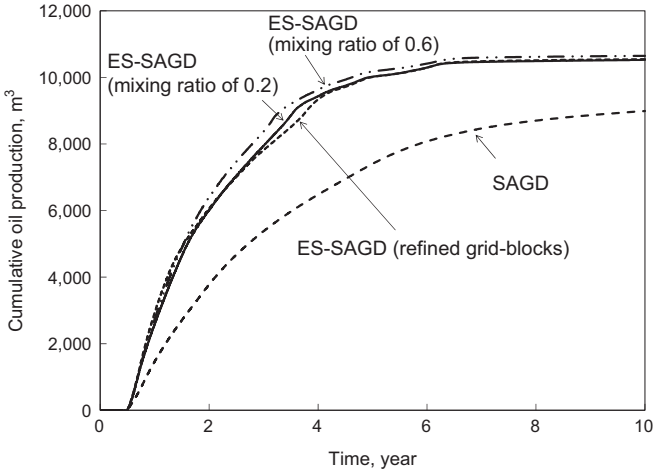

Fig. 4. Cumulative oil recoveries in the SAGD and ES-SAGD simulations given in Section 2. The amount of solvent recovered is not considered for the ES-SAGD plots. The ES-SAGD simulation shows higher oil production rate and more oil recovery that the SAGD simulation. The three ES-SAGD cases compare the effect of using different mixing ratios of oil and solvent to generate *K*-value tables as well as the effect of grid refinement. The effect of the mixing ratio and grid refinement is insignificant on oil recovery prediction in this research.

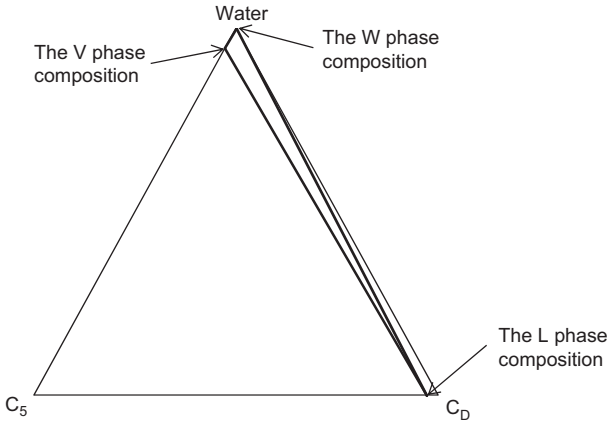

Fig. 5. The tie triangle for the water, C_5, and C_D mixtures at 224.5 °C and 2715 kPa (i.e., conditions inside the chamber).

with refined grid-blocks (0.2 m × 1.0 m × 1.0 m). As shown in Fig. 4, the difference in the oil production curve is insignificant for these simulations.

3. Solvent accumulation near the chamber edge

In ES-SAGD, solvent components are transported efficiently to the chamber edge in the V phase. Fig. 5 presents the tie triangle in composition space for water, C_5, and C_D at 224.5 °C at 2715 kPa based on the *K*-values generated in Section 2. Here, only three components are used for simplicity for the illustration. The V phase contains C_5 at a higher concentration than the L phase; i.e., the *K* value of C_5 is greater than 1.0 at these conditions. More importantly, the mobility of the V phase is much higher than that of the L phase. Propagation of solvent components in ES-SAGD should be carefully designed based on the interaction of flow and phase behavior. If solvent components are present at substantially low concentrations in the V phase near the chamber edge, such ES-SAGD will show oil recovery similar to that of the conventional SAGD at the costs associated with solvent coinjection.

Fig. 6 shows the distributions of the W phase and the C_5 mole fraction in the L phase at 27 months. The V phase releases its latent heat near the chamber edge resulting in accumulation of the W phase there. The C_5 component transported mainly in the V phase

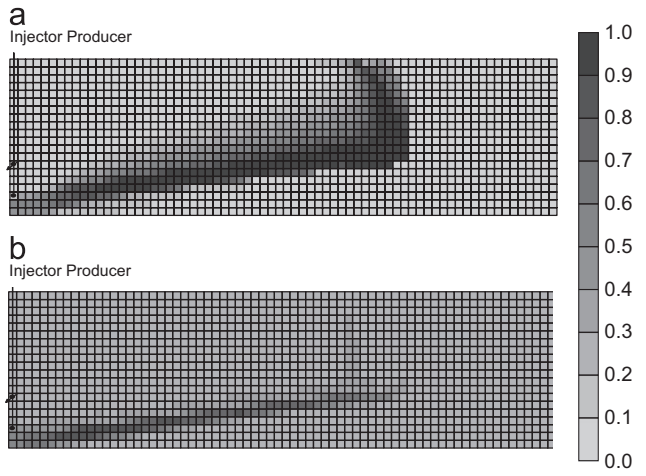

Fig. 6. Gravity segregation of condensed water and solvent banks at 27 months in the ES-SAGD simulation. (a) Distribution of the C_5 mole fraction in the L phase, and (b) distribution of the W phase saturation.

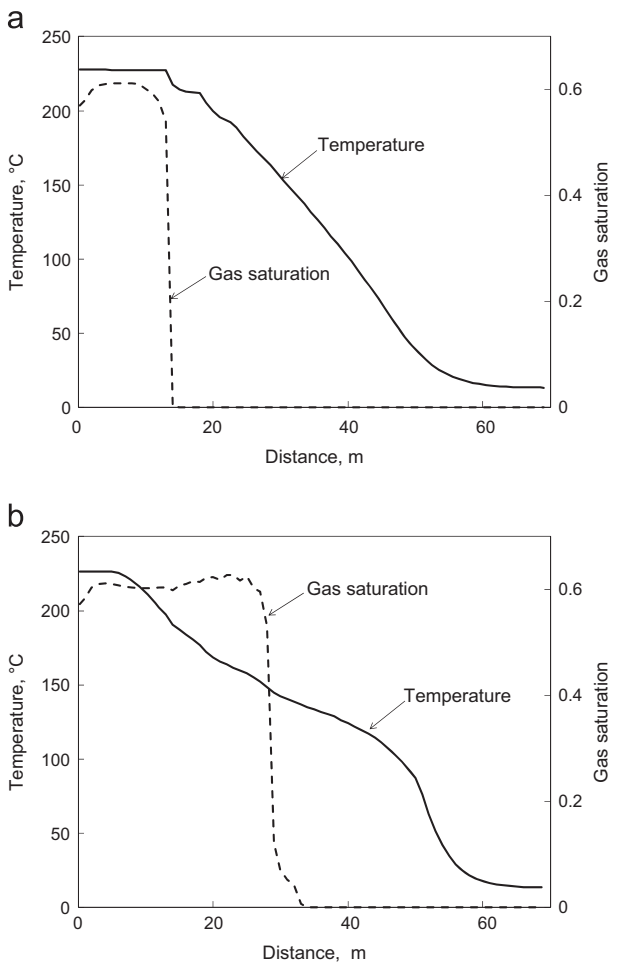

Fig. 7. Distribution of the V phase saturation and temperature in the 14th row at 27 months in (a) the SAGD simulation, and (b) the ES-SAGD simulation. The chamber edge is defined where the V phase saturation becomes zero. The chamber-edge temperature for the ES-SAGD simulation is 87 °C lower than that for the SAGD simulation.

condenses near the chamber edge, where the concentration of C_5 becomes significantly high in the L phase. A C_5 concentration of 0.95 in the L phase is observed in the simulation. Gravity segregation is observed for the condensed water and C_5 along the chamber edge. That is, the hot W phase flows below the C_5-rich L phase in the simulation studied.

Existence of the solvent component can significantly alter the thermodynamic equilibrium conditions near the chamber edge (Dong, 2012; Keshavarz et al., 2013a, 2013b). For this reason, the ES-SAGD exhibits temperature distributions that are different from those in the conventional SAGD. Fig. 7(a) and (b) shows the temperature and V phase saturation profiles of the SAGD and ES-SAGD simulations for the 14th row from the top of the reservoir model (i.e., 6 m from the reservoir bottom) at 27 months. In this research, the chamber edge is defined where the V-phase saturation changes to zero. In the SAGD simulation, the temperature is nearly constant when the V phase exists in Fig. 7(a). The V phase releases its latent heat on the steam chamber edge, and temperature decreases in the hot water bank.

The chamber temperature in the ES-SAGD simulation starts decreasing while the V phase is present. The concentration of C_5 in the V phase becomes high in this temperature transition zone inside the chamber. The L phase saturation inside the chamber can be low and even below the S_{or} as will be shown in Section 5. The ES-SAGD simulation shows accumulation of C_5 in the V phase inside the chamber, and in the L phase outside the chamber.

The accumulation of C_5 in the vicinity of the chamber edge in the ES-SAGD simulation causes the chamber-edge temperature to be significantly lower than that in the SAGD simulation (Fig. 7 (a) and (b)). The difference observed is as much as 87 °C. This means that the mobile liquid phases' temperature in the ES-SAGD simulation is significantly lower than that in the SAGD simulation. The most effective solvent dilution will not occur for the oil at the steam injection temperature (227 °C in this study), but for the oil at a much lower temperature (140 °C in this study). A question then arises as to how the ES-SAGD simulation results in a higher oil production rate than the SAGD simulation as given in Fig. 4. This point will be discussed in the subsequent section.

4. Increased oil production rate in ES-SAGD

The histories of bitumen production rates in the SAGD and ES-SAGD simulations are compared in Fig. 8. The production of C_5

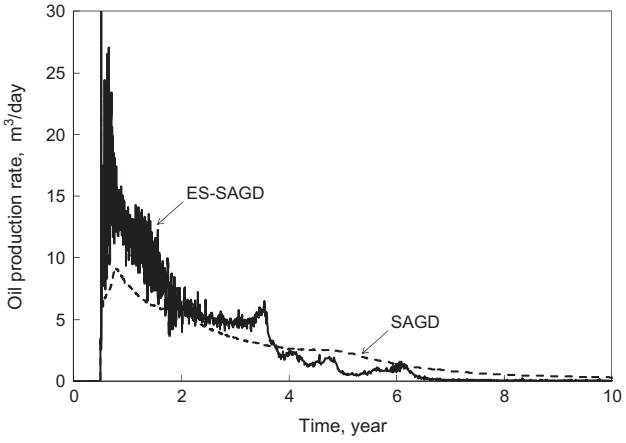

Fig. 8. Oil production rates in the SAGD and ES-SAGD simulations. The production of C_5 as part of oil is excluded for the ES-SAGD simulation. The ES-SAGD simulation exhibits about two times higher oil rate than the SAGD simulation in the early times. The ES-SAGD oil rate becomes lower than the SAGD oil rate after the ES-SAGD chamber reaches the side boundary of the reservoir.

as part of oil is excluded for the ES-SAGD case. Improved oil production rates are observed during the early and intermediate stages in the ES-SAGD simulation, where the average oil production rate of ES-SAGD shows about 50% improvement over that of SAGD. This is comparable to the field performances of solvent–steam coinjection as described in Section 1 and indicates that the current simulation model captures the key mechanisms in an idealized coinjection process. Interpretation of the increased oil rate in ES-SAGD should consider the solvent accumulation and temperature distribution near the chamber edge described in Section 3. A simple analysis is given below as to how the improved oil production rate is achieved in ES-SAGD.

Darcy's law for the L phase in the direction parallel to the chamber edge during SAGD is

$$u_o = -\frac{kk_{ro}}{\mu_o}\frac{\partial \Phi_o}{\partial \eta}, \tag{3}$$

where η is the distance in the direction parallel to the chamber edge. The oil–component molar flux in the L phase j_o [mole/m^2 s] for SAGD is

$$j_o = -\frac{kk_{ro}}{\mu_o}\frac{\partial \Phi_o}{\partial \eta}\rho_o, \tag{4}$$

where ρ_o is the molar density of the L phase. Similarly for the oil–component molar flux in the L phase j_o' for ES-SAGD,

$$j_o' = -\frac{kk_{ro}'}{\mu_o'}\frac{\partial \Phi_o'}{\partial \eta}\rho_o' x_o'. \tag{5}$$

The L phase in ES-SAGD consists of solvent and reservoir oil components. Eq. (5) represents the mole fraction of reservoir oil components in the L phase for ES-SAGD as x_o'. It is 1.0 for the conventional SAGD. The μ_o' and ρ_o' terms are the viscosity and molar density of the L phase as an oil–solvent mixture, respectively. Assuming the same potential gradient for Eqs. (4) and (5), the ratio of the oil component molar flux in ES-SAGD to that in SAGD is

$$\frac{j_o'}{j_o} = \frac{k_{ro}'}{k_{ro}}\frac{\mu_o}{\mu_o'}\frac{\rho_o'}{\rho_o}x_o'. \tag{6}$$

Eq. (6) has four terms that affect the oil–component molar flux ratio: the relative permeability ratio, the viscosity ratio, the molar density ratio, and the oil–component mole fraction in the L phase. Using Eq. (6), one can identify the individual contributions of the four terms at different distances from the chamber edge. The product of the first two terms represents the relative mobility ratio of the draining L phase in ES-SAGD to that in SAGD. The product of the last two terms represents the ratio of the reservoir oil (C_D) contents per unit volume of the draining L phase in these two processes. Eq. (6) also indicates that improved oil production rate simulated for ES-SAGD depends on how physical properties, like relative permeabilities and phase viscosities, are modeled in the simulation.

The relative permeability ratio k_{ro}'/k_{ro} depends on the L phase saturations for the SAGD and ES-SAGD cases, which vary with the distance from the chamber edge. Fig. 9 shows that the L phase saturation distribution of the ES-SAGD simulation is significantly different from that of the SAGD simulation. In the ES-SAGD simulation, the L phase saturation is increased in the condensed C_5 bank near the chamber edge, but it is reduced in the hot water bank. At 15 m from the chamber edge, the relative permeability ratio shows a minimum due to the limited L phase saturation in the ES-SAGD hot water bank. In the SAGD simulation, the hot water bank exists just outside the chamber edge. Thus, the L phase saturation varies from the residual oil saturation at the chamber edge to the initial L phase saturation beyond the hot water bank (Sharma and Gates, 2010).

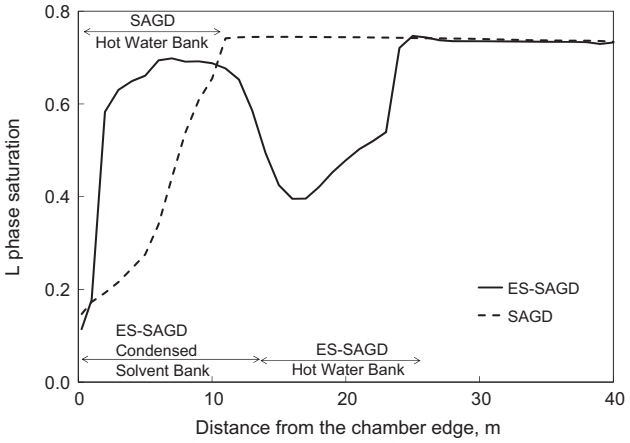

Fig. 9. Distribution of the L phase saturation at different distances from the chamber edge in the 14th row at 27 months in the ES-SAGD and SAGD simulations.

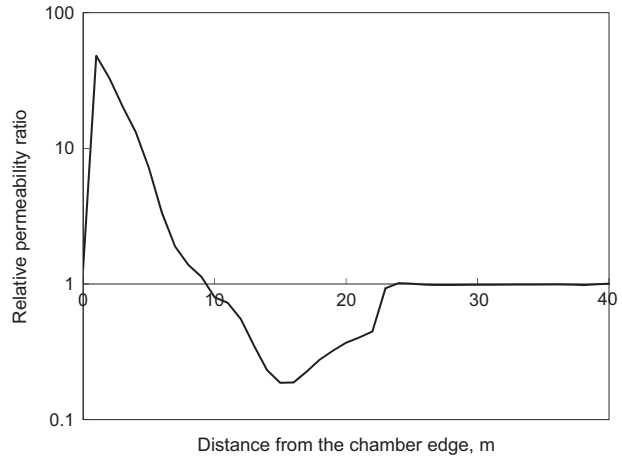

Fig. 10. Relative permeability ratio at different distances from the chamber edge in the 14th row at 27 months. The relative permeability ratio is defined in Section 4.

Fig. 10 shows the relative permeability ratio at different distances from the chamber edge. In ES-SAGD, the gravity segregated flow of hot water and condensed solvent banks raises the L phase saturation just outside the chamber edge. Therefore, the L phase relative permeability in this region is much higher in ES-SAGD than in SAGD (0–9 m in Fig. 10). The relative permeability ratio is decreased in the water bank (9–23 m in Fig. 10).

The viscosity ratio μ_o/μ_o' given in Fig. 11 is controlled mainly by the temperature distribution and solvent dilution. As explained in Section 3, the chamber edge temperature in ES-SAGD can be much lower than in SAGD due to accumulation of solvent along the chamber edge. In the region further than 22 m, the L phase viscosity is higher in ES-SAGD as a result of the lower chamber edge temperature. However, accumulation of condensed solvent just outside the chamber edge can reduce the viscosity of the L phase to two orders of magnitude smaller values. The relative mobility ratio $(k_{ro}'/k_{ro})(\mu_o/\mu_o')$ is shown in Fig. 12, which exhibits combined effects of the relative permeability and viscosity ratios.

Fig. 13 shows the oil-component (i.e., C_D) mole fraction in the L phase outside the chamber edge in the 14th row from the top of the reservoir model. Due to solvent accumulation near the chamber edge, the oil-component mole fraction just outside the chamber edge can be as small as 0.05. This shows that the amount of the oil component can be substantially small in the mobile oil zone.

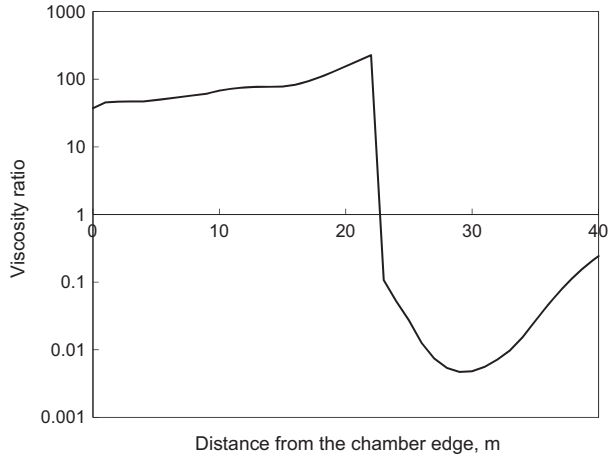

Fig. 11. Viscosity ratio at different distances from the chamber edge in the 14th row at 27 months. The viscosity ratio is defined in Section 4.

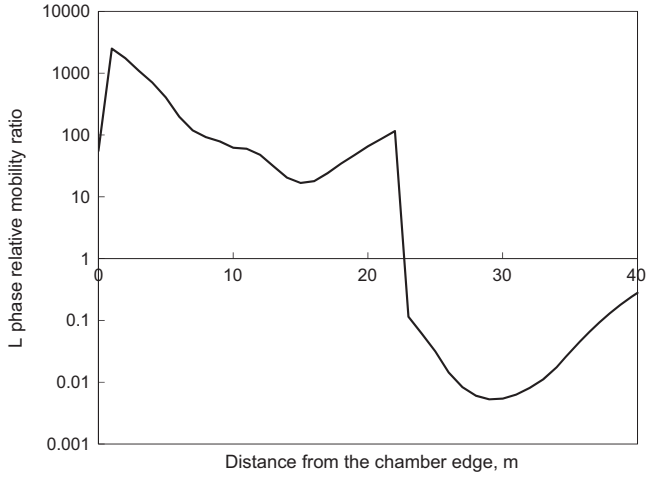

Fig. 12. Relative mobility ratio at different distances from the chamber edge in the 14th row at 27 months. The relative mobility ratio is defined in Section 4.

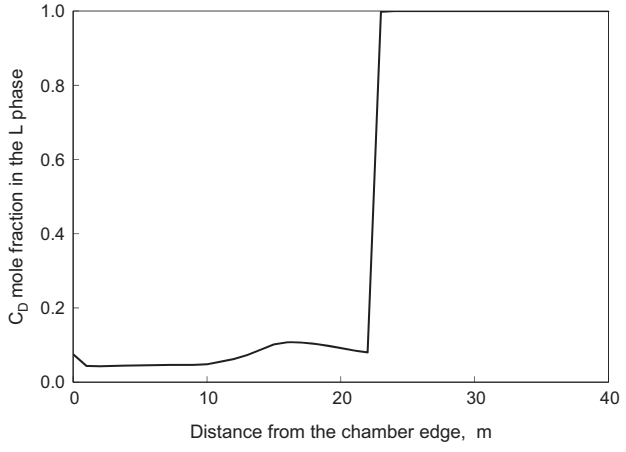

Fig. 13. The C_D mole fraction in the L phase at different distances from the chamber edge in the 14th row at 27 months in the ES-SAGD simulation. It can be as small as 0.05 in the condensed-C_5 bank located 0–15 m outside the chamber edge.

Fig. 14 shows the L phase molar density ratio ρ_o'/ρ_o. Mixing of the condensed solvent with the reservoir oil reduces the mass density of the oleic phase, but it increases the molar density according to Eq. (2). The reason is that the coinjected solvent has a lower mass density and a higher molar density compared to the

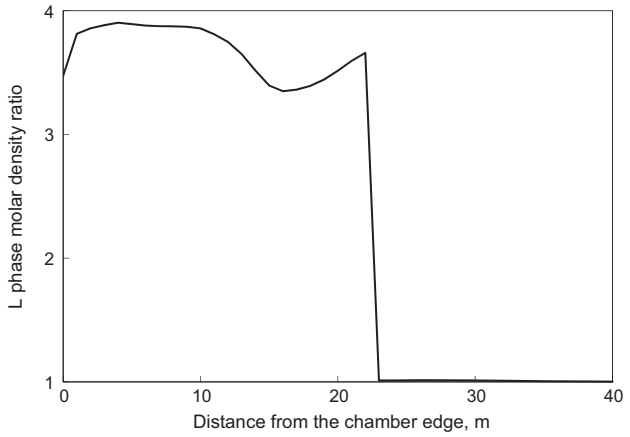

Fig. 14. Molar density ratio at different distances from the chamber edge in the 14th row at 27 months. The molar density ratio is defined in Section 4.

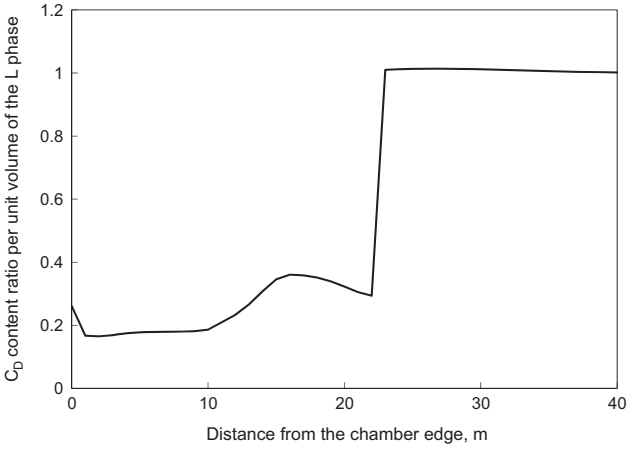

Fig. 15. Reservoir oil (C_D) content ratio per unit volume of the L phase at different distances from the chamber edge in the 14th row at 27 months. The oil content ratio is defined in Section 4.

original reservoir oil. The ratio of the reservoir oil contents per unit volume of the L phase defined as $(\rho_o'/\rho_o)\,x_o'$ is shown in Fig. 15.

Finally, the ratio of the oil component molar flux in ES-SAGD to that in SAGD is given in Fig. 16 based on Eq. (6). The denominator of Eq. (6) becomes less significant with the distance from the chamber edge. That is, the molar flux ratio has more significant impact on the ES-SAGD oil production rate in the region closer to the chamber edge. There are two distinct regions in Fig. 16 as follows:

Region 1 (0–23 m): At distances up to 10 m, ES-SAGD shows the oil–component molar flux that is significantly increased, compared to SAGD. Accumulation of condensed solvent in this region in ES-SAGD not only reduces the viscosity of the L phase (Fig. 11), but also results in higher relative permeability to the L phase (Fig. 10). The descending trend of the curve follows the same trend of the relative permeability ratio. The mixing of solvent and oil in this region is caused by molecular diffusion and enhanced by convection as discussed in Garmeh and Johns (2010). The convection here is mainly the gravity drainage along the chamber edge. The transverse dispersion associated with the gravity drainage is likely the main driving force for the spatial distribution of the condensed solvent beyond the chamber edge (Keshavarz et al., 2013a, 2013b).

Region 2 (23–40 m): In this region, the difference in the temperature profiles (Fig. 7) becomes the controlling parameter. The relative mobility ratio is higher for SAGD due to its lower oil

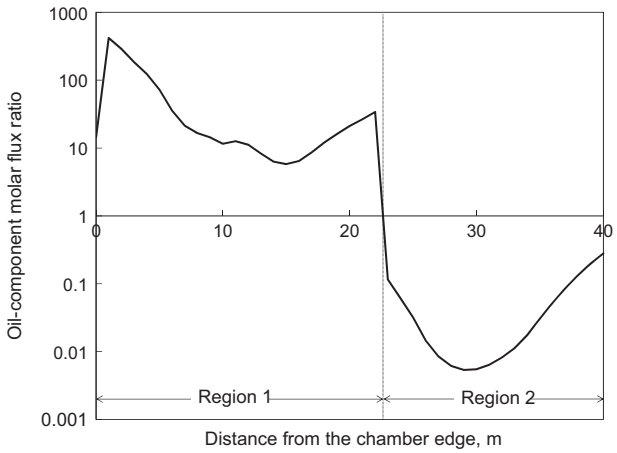

Fig. 16. Oil–component molar flux ratio at different distances from the chamber edge in the 14th row at 27 months. The oil–component molar flux ratio is defined in Eq. (6).

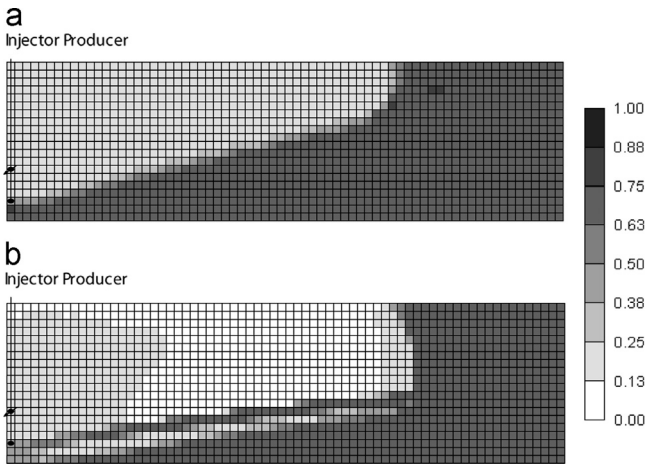

Fig. 17. Distribution of the L phase saturation in (a) the SAGD simulation, and (b) the ES-SAGD simulation at 27 months. The L phase saturation near the ES-SAGD chamber edge is substantially lower than the residual oil saturation 0.13. The L phase saturation in the SAGD chamber and in the near-well region of the ES-SAGD chamber is about 0.13.

viscosity in this region. The ascending trend of the curve towards unity near 40 m indicates that heat effects are diminishing.

The analysis in this section shows that increased oil production rate in ES-SAGD may result from the combined effects of bitumen dilution with solvent, solvent accumulation, and temperature distribution near the chamber edge. In this research, the ES-SAGD simulation results in about 50% improvement in the average oil production rate compared to SAGD simulation in the early to intermediate stages of the process (Fig. 8). The faster oil recovery results in faster propagation of the ES-SAGD chamber. The lower oil production rates of ES-SAGD compared to SAGD that can occur in the late stages of the process is due to the fact that the ES-SAGD chamber has reached the side boundary of the reservoir.

5. Displacement efficiency enhanced by ES-SAGD

In this section, we investigate how ES-SAGD can achieve oil saturation lower than the residual saturation on the basis of phase equilibrium in composition and temperature space in numerical simulation. Fig. 4 shows that the ES-SAGD simulation results in 27% more oil recovery at 6 years, and 17% more oil recovery at 10 years, compared to the SAGD simulation. The enhanced oil recovery is a direct result of faster propagation of the ES-SAGD chamber and enhanced displacement efficiency in the chamber as shown in Fig. 17. Oil saturation in the SAGD simulation studied cannot be lower than the residual saturation of 0.13. In the ES-SAGD simulation, oil saturation in the chamber can be much lower than the residual saturation. An oil saturation as low as 0.001 is observed in the region away from the well pair. In the near-well region of the ES-SAGD simulation, oil saturation is similar to that in the SAGD simulation.

As mentioned in Jha et al. (2013), there are several attempts in the literature to model the reduced residual oil saturations observed in steam–solvent coinjection experiments. They include the use of small residual oil saturations to gas, composition-dependent residual oil saturations, and modified end-point saturations to capture IFT reduction in coinjection simulation (Gates, 2007; Ardali et al., 2011; Yazdani et al., 2011). Such manipulations of relative permeabilities, however, still need further investigations. In this study, we demonstrate that such oil saturation reduction can be explained by considering interaction of solvent accumulation, temperature variation, and phase equilibrium in the ES-SAGD simulation.

We use three components in the ES-SAGD simulation in this section. They are water, C_5, and C_D; i.e., the reservoir oil in this simulation is dead oil. The solvent compound coinjected is C_5. The properties of C_D and C_5 are given in Tables 2 and 3. Three is the minimum number of components required to explain enhanced displacement efficiency in ES-SAGD. The ternary system also allows for visual illustration of the mechanisms using simple ternary diagrams.

In an ES-SAGD chamber (Fig. 17), there are three equilibrium phases, the L, V, and W phases. The V phase disappears at the chamber edge as illustrated in Fig. 7. Beyond the chamber edge, there are two liquid phases, the L and W phases. Temperature decreases with the distance from the well pair. A significant change in temperature occurs near the chamber edge as given in Fig. 7. ES-SAGD also involves significant composition variation resulting from accumulation of condensed water and solvent near the chamber edge as explained in Section 3.

Fig. 18(a)–(e) and Table 4 present overall compositions, phase compositions, phase amounts, pressure, and temperature at gridblock (47, 7) at different times in the ES-SAGD simulation using water, C_5, and C_D. Gridblock (1, 1) is defined at the left-top gridblock. The bold point in each diagram represents the overall composition in that gridblock. Fig. 18 (a) shows that the initial reservoir fluid composition lies on a tie line between the L and W phases, which corresponds to the water–C_D edge of the diagram. The C_5 component does not exist in the gridblock yet.

Significant accumulation of condensed C_5 near the chamber edge results in a gravity segregation of the condensed W phase and the solvent-rich L phase. The gridblock is affected initially by the condensed W phase (Fig. 18(b)), and then by the solvent-rich L phase (Fig. 18(c)). The overall mole fraction of water is as high as 0.95 in Fig. 18(b) as also given in Table 4. The mole fraction of C_5 also increases to 0.04, which swifts the equilibrium L phase composition towards the C_5 vertex along the C_5–C_D edge. In Fig. 17(c), the L phase becomes significantly rich in C_5. The C_5 mole fraction is as high as 0.97 in the L phase. This occurs because the C_5 overall composition increases from 0.04 to 0.2 near the water–C_5 edge while moving from Fig. 18(b) to 18(c). Since the overall composition in ES-SAGD varies at high concentrations of the water component, the

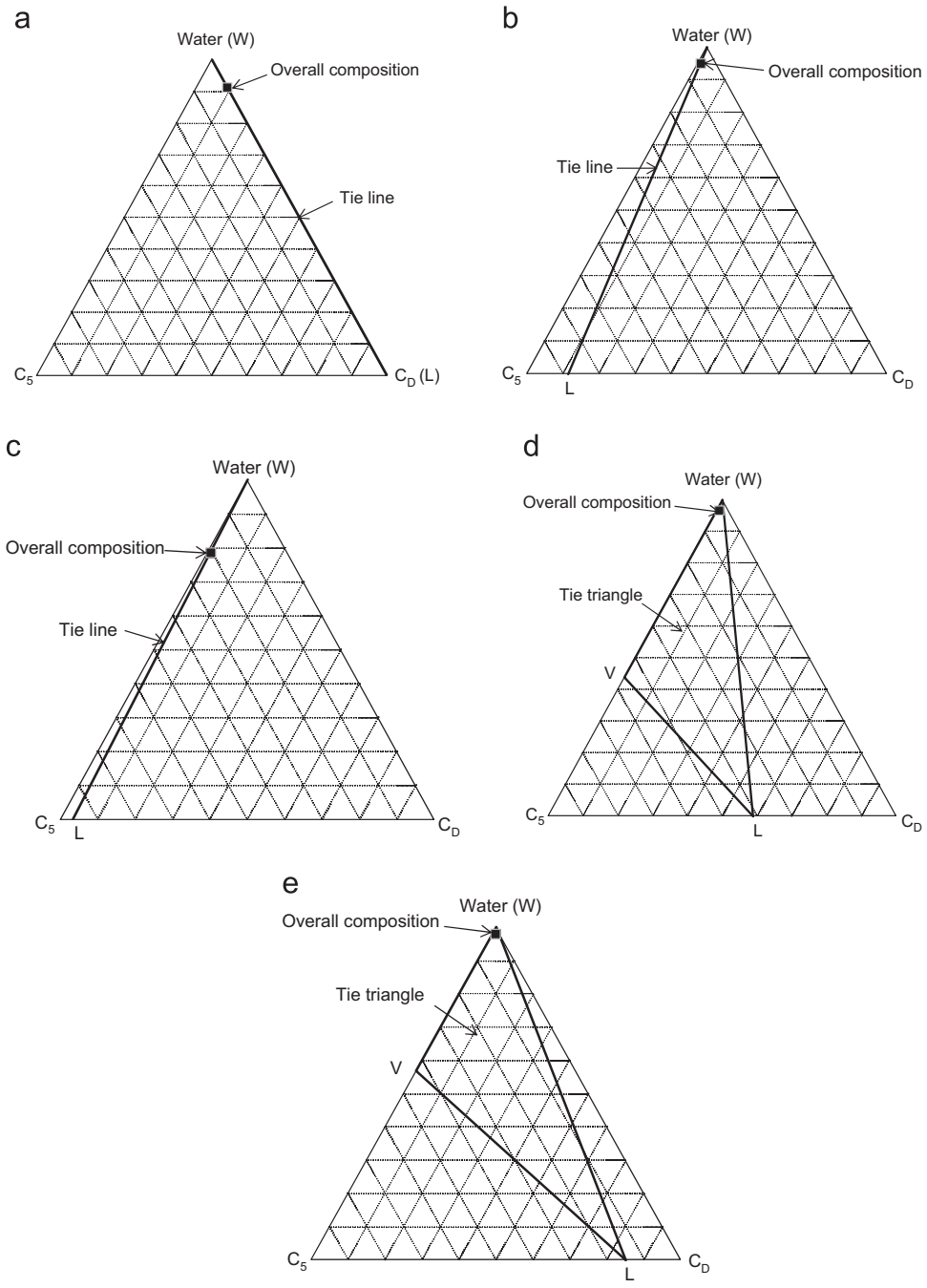

Fig. 18. Overall composition and phase equilibrium at gridblock (47, 7) in the ES-SAGD simulation using the water, C_5, and C_D components. Pre-heating period (6 months) is excluded in the reported times. (a) 6 months from the start of the three-component ES-SAGD simulation. Gridblock (47, 7) is not affected by C_5. (b) 12.5 months from the start of the three-component ES-SAGD simulation. Gridblock (47, 7) is in the condensed water bank. (c) 15 months from the start of three-component ES-SAGD simulation. Gridblock (47,7) is in the condensed C_5 bank. (d) 18 months from the start of the three-component ES-SAGD simulation. Gridblock (47, 7) is just inside the ES-SAGD chamber. The L phase in the previous figure is split into the V and L phases in the presence of the invariant W phase. (e) 2 years from the start of the three-component ES-SAGD simulation. Gridblock (47, 7) is inside the ES-SAGD chamber. The V and L phases become less rich in C_5.

equilibrium L phase composition is sensitive to variation of the overall composition.

After this stage, the ES-SAGD chamber contains the gridblock, where the three phases, L, V, and W, are present. During this phase transition, the L phase saturation becomes lower than the residual oil saturation. The L phase saturation is 0.6227 for Fig. 18(c) and 0.0534 for Fig. 18(d), and the residual saturation is 0.13 in this simulation. The reduction in the L phase saturation occurs because the L phase in Fig. 18(c) splits into the V and L phases in Fig. 18(d) in the presence of the invariant W phase. The small L phase saturation in Fig. 18(d) directly comes from the geometric relationship between the overall composition and the L phase composition. This implies that the L phase has moved away from the C_5 vertex, while the overall composition is located near the water–C_5 edge. This geometric relationship results in a small L phase mole fraction, and therefore a small L phase saturation, which is a function of molar densities and mole fractions of the equilibrium phases. From this point on, the V and L phases become less rich in C_5 as illustrated in Fig. 18 (d) and (e).

Table 4
Overall composition, phase amounts, pressure, and temperature for Fig. 18(a)–(e).

Properties	(a)	(b)	(c)	(d)	(e)
Overall mole fraction of water	0.9145	0.9523	0.7873	0.9688	0.9824
Overall mole fraction of C_D	0.0855	0.0055	0.0071	0.0053	0.0060
Overall mole fraction of C_5	0.0000	0.0422	0.2057	0.0259	0.0116
Mole fraction of the W phase	0.9145	0.9523	0.7873	0.9514	0.9525
Mole fraction of the L phase	0.0855	0.0477	0.2127	0.0089	0.0070
Mole fraction of the V phase	0.0000	0.0000	0.0000	0.0397	0.0405
Saturation of the W phase	0.2580	0.6794	0.3273	0.2913	0.2645
Saturation of the L phase	0.7420	0.3206	0.6727	0.0534	0.0479
Saturation of the V phase	0.0000	0.0000	0.0000	0.6553	0.6876
Temperature (°C)	13.1	121.8	160.4	185.4	211.0
Pressure (kPa)	2153	2666	2667	2669	2689

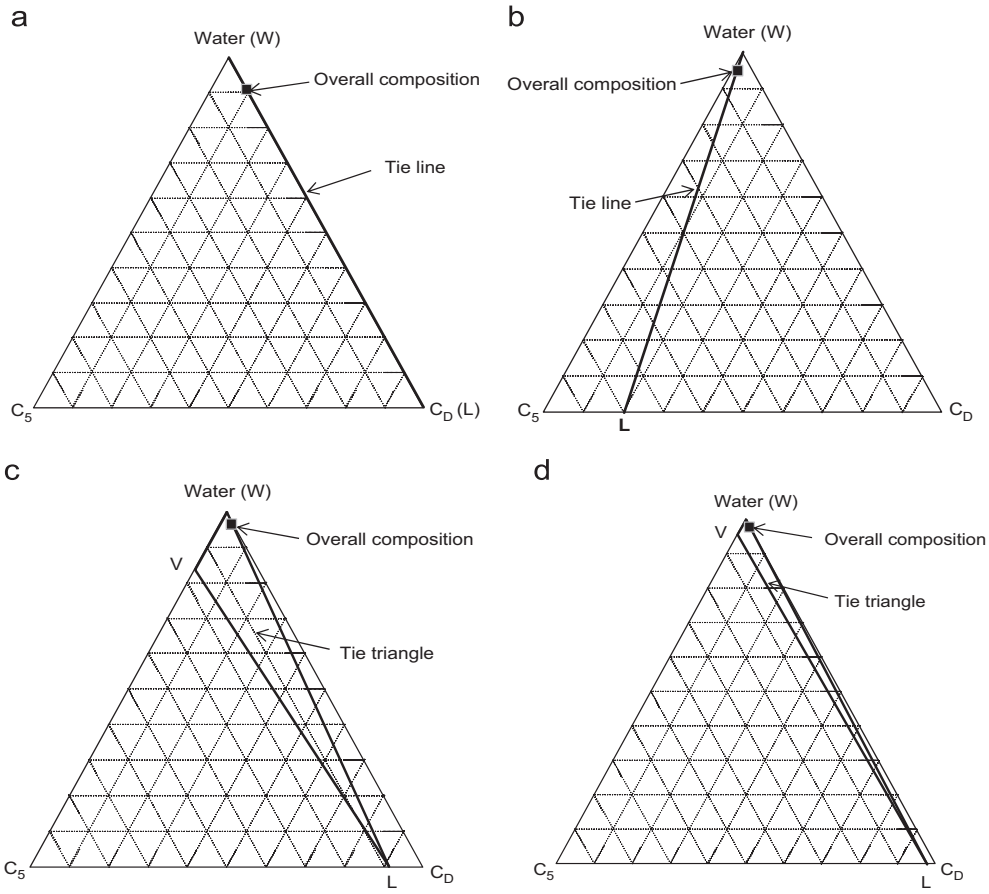

Fig. 19. Overall composition and phase equilibrium at gridblock (9, 12) in the ES-SAGD simulation using the water, C_5, and C_D components. Pre-heating period (6 months) is excluded in the reported times. (a) 2 months from the start of the three-component ES-SAGD simulation. Gridblock (9, 12) is not affected by C_5. (b) 3.5 months from the start of the three-component ES-SAGD simulation. The C_5 concentration in gridblock (9, 12) cannot be as high as in gridblock (47, 7) given in Fig. 18. (c) 4 months from the start of the three-component ES-SAGD simulation. The C_D concentration in the tie triangle is not as small as in gridblock (47, 7) given in Fig. 18, resulting in a higher L phase mole fraction. (d) 18 months from the start of the three-component ES-SAGD simulation. The C_D concentration in the tie triangle is not as small as in gridblock (47, 7) given in Fig. 18, resulting in a higher L phase mole fraction.

The mechanism described above for reduction of the L phase saturation requires significant accumulation of solvent and phase transition near the chamber edge. Depending on how fast the condensed C_5 is removed from the chamber edge as part of the draining L phase, it starts accumulating in this region.

At the early stage of the process, significant reduction in the L phase saturation cannot be expected because solvent accumulation is not considerable. This explains why the region with reduced L phase saturations exists closer to the chamber edge in Fig. 17. The gridblocks in this region are affected by the condensed C_5-rich bank when solvent accumulation has become considerable at the chamber edge.

Fig. 19(a)–(d) along with Table 5 illustrates the phase behavior in gridblock (9, 12), which is closer to the well pair than gridblock (47, 7) discussed above. This gridblock does not show L phase saturations lower than the residual saturation throughout the simulation. The difference between Figs. 18 and 19 is that the overall mole fraction of C_5 in Fig. 19 does not go beyond 0.04, even when the gridblock is located in the condensed C_5-rich bank. More time is required to accumulate a sufficient amount of C_5 (e.g., a

Table 5
Overall composition, phase amounts, pressure, and temperature for Fig. 19(a)–(d).

Properties	(a)	(b)	(c)	(d)
Overall mole fraction of water	0.9111	0.9512	0.9671	0.9808
Overall mole fraction of C_D	0.0889	0.0098	0.0268	0.0173
Overall mole fraction of C_5	0.0000	0.0390	0.0061	0.0019
Mole fraction of the W phase	0.9111	0.9512	0.9490	0.9477
Mole fraction of the L phase	0.0889	0.0488	0.0294	0.0177
Mole fraction of the V phase	0.0000	0.0000	0.0216	0.0346
Saturation of the W phase	0.2501	0.6326	0.3115	0.2612
Saturation of the L phase	0.7499	0.3674	0.2469	0.1299
Saturation of the V phase	0.0000	0.0000	0.4416	0.6089
Temperature (°C)	30.4	163.8	217.6	225.0
Pressure (kPa)	2698	2696	2696	2707

Table 6
Overall composition, phase amounts, pressure, and temperature for Fig. 20(a)–(c).

Properties	(a)	(b)	(c)
Overall mole fraction of water	0.9147	0.9779	0.9823
Overall mole fraction of C_D	0.0853	0.0221	0.0177
Mole fraction of the L phase	0.0853	0.0221	0.0177
Mole fraction of the V and W phases	0.9147	0.9779	0.9823
Saturation of the W phase	0.2586	0.6222	0.2567
Saturation of the L phase	0.7414	0.3778	0.1300
Saturation of the V phase	0.0000	0.0000	0.6133
Temperature (°C)	13.2	226.9	227.3
Pressure (kPa)	2142	2681	2701

concentration of 0.2) depending on phase behavior of the water/bitumen/solvent mixtures. Therefore, the overall composition in Fig. 19 does not become sufficiently close to the water–C_5 edge. In this case, the phase transition between two to three phases at the chamber edge cannot reduce the L phase saturation below the residual saturation.

Table 6 shows the variations in the overall composition, phase amounts, pressure, and temperature at gridblock (25, 5) for the SAGD simulation with water and C_D. There is no C_5 injected in this simulation. The composition variation occurs only along the water–C_D edge of the ternary diagrams in Fig. 20, which corresponds to the tie line representing either the L–W or L–V equilibrium. The series of ternary diagrams present that the overall mole fraction of the water component increases as soon as the cell is affected by the condensed water bank at the chamber edge. The overall composition remains more or less unchanged after this time.

The analysis in this section is based on a dead oil reservoir with three components. The mechanism identified is also valid for the multi-component live-oil case presented in Section 6.

6. Verification of the mechanisms using a multi-component reservoir oil

This section presents the verification of the identified mechanisms by use of a multi-component live oil. A simple phase behavior model is created for the live oil by combining the Athabasca dead bitumen with some non-condensable gas components and intermediate components.

Component grouping is used to reduce the computational costs; i.e., components C_1, C_2, and C_3 are grouped into pseudo-component 1 (PC1); C_4, C_5 and C_6 into pseudo-component 2 (PC2); and, C_7, C_8 and C_9 into pseudo-component 3 (PC3). Table 7 shows the resulting composition of the live oil and the properties of the pseudo-components. Other properties of the dead bitumen (the C_D component) were described in Section 2.

The STARS simulator (Computer Modeling Group 2013) is used to run the simulations. Properties of the reservoir model are similar to those described in Section 2. C_5 is coinjected with steam at a constant concentration of 2 mol% for the ES-SAGD process. *K*-values are independent of the composition in each simulation case. However, three different mixing ratios 0.2, 0.5 and 0.8 for C_5/live-oil were used to prepare three different *K*-value tables. Fig. 21 compares oil production histories simulated for these three ES-SAGD cases and the SAGD case. An improvement of more than 50% in the average oil drainage rate is observed during the first 5 years of the project when C_5 is coinjected with steam. Use of a lower solvent/bitumen mixing ratio for preparation of *K*-value tables results in more conservative predictions of oil production rates for the cases studied in this section.

Fig. 22 compares the profiles of residual oil saturation inside the SAGD and ES-SAGD chambers after 27 months from the start of the projects. Fig. 22 confirms that the residual oil saturation inside the ES-SAGD chamber can be substantially lower than that in the SAGD chamber in the regions that have experienced a sufficient amount of solvent accumulation.

Numerical simulations of C_5-steam coinjection were also conducted by use of composition dependent *K*-values that are available in the STARS simulator. C_5 was selected as the key component with overall mole fractions of 10%, 50% and 90%. Three *K*-value tables were generated for each component. The simulations, however, were terminated after simulating about 1 year of the coinjection process due to non-convergence. Therefore, their results are not presented. However, it was observed that the identified mechanisms in this work remained valid until the simulations stopped from proceeding.

Existence of solution gas in the chamber did not alter the identified mechanisms in the simple numerical simulations studied. Further research is required to have more general understanding of the oil recovery mechanisms in coinjection processes, which involve 3-D non-isothermal multi-component fluid flow in heterogeneous porous media.

7. Conclusions

A detailed simulation study was conducted on ES-SAGD mechanisms. Explanations were given as to how ES-SAGD can achieve higher oil production rate and displacement efficiency than SAGD. The conclusions are as follows:

1. ES-SAGD can efficiently transport its solvent compounds to the chamber edge using the gaseous phase. Accumulation of the solvent component occurs in the gaseous phase inside the chamber edge, while it occurs in the oleic phase outside the chamber edge. The solvent accumulation in the early stage of ES-SAGD is not sufficient to exhibit the advantage of ES-SAGD over SAGD in terms of local displacement efficiency. The solvent accumulation in

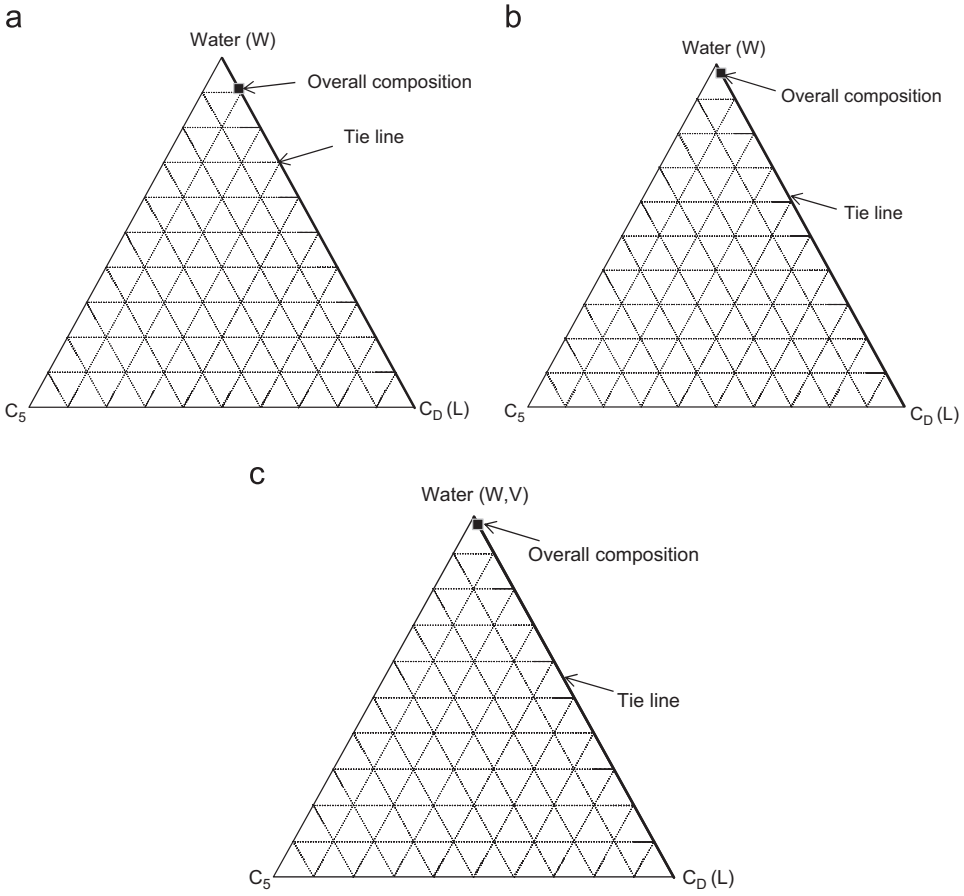

Fig. 20. Overall composition and phase equilibrium at gridblock (25, 5) in the SAGD simulation using the water and C_D components (without the C_5 component). Pre-heating period (6 months) is excluded in the reported times. (a) 4 months from the start of the two-component SAGD simulation. (b) 11 months from the start of the two-component SAGD simulation. (c) 2 years from the start of the two-component SAGD simulation.

Table 7
Overall composition and the properties of the live bitumen used in Section 6.

Component	Mole fraction	Molecular weight, kg/kg mole	T_c, °C	P_c, kPa	Acentric factor
C_D	0.90	594.6	817.75	785.98	1.3611
PC1	0.05	30.07	21.13	4699.37	0.0860
PC2	0.03	72.15	196.19	3361.01	0.2467
PC3	0.02	114.2	295.58	2501.50	0.3963

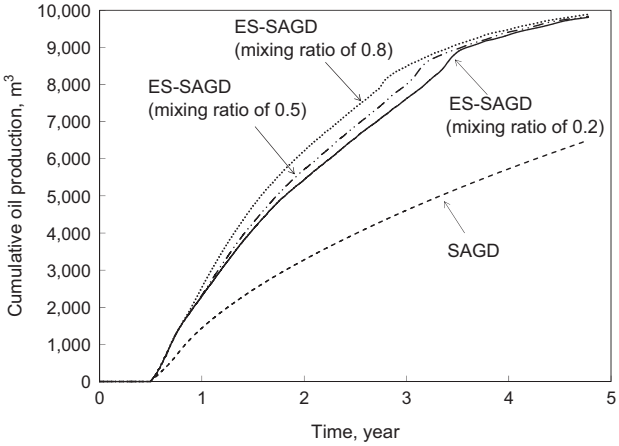

Fig. 21. Cumulative oil recoveries in the SAGD and ES-SAGD simulations given in Section 6. The amount of solvent recovered is not considered for the ES-SAGD plots. The ES-SAGD simulation shows higher oil production rate and more oil recovery than the SAGD simulation. Three ES-SAGD cases show the effect of using different solvent–live oil mixing ratios for generating *K*-value tables. Coinjection of C_5 has resulted in more than 50% improvement in the average oil production rate during the first five years of the project.

the vicinity of the chamber edge can result in a chamber-edge temperature that is significantly lower than that in SAGD.

2. ES-SAGD can achieve oil saturations lower than the residual saturation in the chamber. The oil saturation reduction results mainly from two processes: (1) solvent accumulation in the oleic phase outside the chamber edge, and (2) phase transition near the chamber edge (i.e., V–L–W inside and L–W outside the chamber edge). The solvent accumulation lowers the oil–component concentrations. The diluted oil is then redistributed in the gaseous and oleic phases in the presence of the water phase during the phase transition. The concentration of the oil component is high in the equilibrium oleic phase. However, the amount of the oleic phase can be significantly small, resulting in low oil saturations in the ES-SAGD chamber. It was observed that the ultimate oil recovery of ES-SAGD is approximately 20% greater than that of SAGD in this research.

3. The difference between the oil production rate in ES-SAGD and that in SAGD depends mainly on three factors; i.e., solvent accumulation, temperature distribution, and bitumen dilution with solvent near the chamber edge. In the simulation cases studied, ES-SAGD exhibited more than 50% faster oil production than SAGD during the early to intermediate stages of the process.

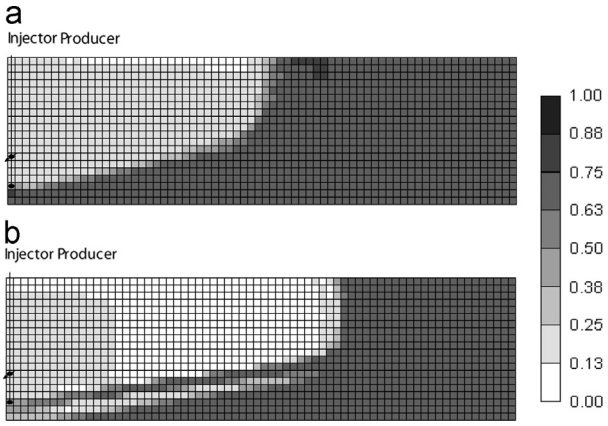

Fig. 22. Distribution of the L phase saturation at 2.7 years in (a) the SAGD simulation, and (b) the ES-SAGD simulation presented in Section 6. The L phase saturation near the ES-SAGD chamber edge is substantially lower than the residual oil saturation 0.13. The L phase saturation in the SAGD chamber and in the near-well region of the ES-SAGD chamber is about 0.13.

Acknowledgments

A partial support for this research was obtained from the third author's (TB) NSERC Industrial Research Chair in Unconventional Oil Recovery (industrial partners are Schlumberger, CNRL, SUNCOR, Petrobank, Sherritt Oil, and APEX Eng.). The second author (RO) gratefully acknowledges a partial financial support from Natural Sciences and Engineering Research Council of Canada (NSERC) for this research.

References

Akbarzadeh, K., Sabbagh, O., Beck, J., Sverck, W.Y., Yarranton, H.W., 2004. Asphaltene Precipitation from Bitumen Diluted With n-Alkanes, Paper CIPC2004-026 Presented at the Petroleum Society's Canadian International Petroleum Conference, Calgary, Alberta, Canada, 8–10 June.

Ardali, M., Mamora, D.D., Barrufet, M., 2011. Experimental Study of Coinjection of Potential Solvents with Steam to Enhance SAGD Process. Paper SPE 144598 Presented at the SPE Western North American Regional Meeting, Anchorage, Alaska, USA, May 7–11.

Badamchizadeh, A., Kohse, B.F., 2011. Modeling of Asphaltene Precipitation Due to Steam and n-Alkane Co-injection in the ES-SAGD Process. Paper CSUG/SPE 149411 Presented at the Canadian Unconventional Resources Conference, Calgary, Alberta, Canada, November 15–17.

Butler, R.M., 1997. Thermal Recovery of Oil and Bitumen. Blackbook series, GravDrain Inc., Calgary, Alberta.

Computer Modeling Group (CMG) Ltd. STARS User Manual. Version 2011. Calgary, Alberta, Canada, 2011 and 2013.

Das, S.K., Butler, R.M., 1998. Mechanism of the vapor extraction process for heavy oil and bitumen. J. Pet. Sci. Eng. 21 (1–2), 43–59.

Deng, X., Huang, H., Zhao, L., Law, D.H.-S., Nasr, T.N., 2010. Simulating the ES-SAGD process with solvent mixture in Athabasca reservoirs. J. Can. Pet. Technol. 49 (1), 38–46.

Dong, L., 2012. Effect of vapor–liquid phase behavior of steam-light hydrocarbon systems on steam assisted gravity drainage process for bitumen recovery. Fuel 95, 159–168.

Edmunds, N.R., Haston, J.A., Best, D.A., 1989. Analysis and implementation of the steam assisted gravity drainage process at the AOSTRA UTF. In: Proceedings of the 4th UNITAR/UNDP International Conference on Heavy Crude and Tar Sands, AOSTRA, Edmonton, vol. 4, pp. 223–238.

Garmeh, G., Johns, R.T., 2010. Upscaling of miscible floods in heterogeneous reservoirs considering reservoir mixing. SPE REE 13 (5), 747–763 (SPE-124000-PA).

Gates, I.D., 2007. Oil phase viscosity behavior in expanding-solvent steam-assisted gravity drainage. J. Pet. Sci. Eng. 59 (1–2), 123–134.

Gupta, S., Gittins, S.D., 2006. Christina lake solvent aided process pilot. J. Can. Pet. Technol. 45 (9), 15–18.

Gupta, S., Gittins, S., Picherack, P., 2005. Field implementation of solvent aided process. J. Can. Pet. Technol. 44 (11), 8–13.

Haghighat, P., Maini, P.P., 2008. Role of asphaltene precipitation in VAPEX process. In: Proceedings of the Canadian International Petroleum Conference/SPE Gas Technology Symposium 2008 Joint Conference, Calgary, Alberta, Canada, 17–19 June.

Hosseininejad Mohebati, M., Maini, B.B., Harding, T.G., 2010. Numerical evaluation of adding hydrocarbon additives to steam in SAGD process. J. Can. Pet. Technol. 49 (9), 42–53.

Farouq Ali, S.M., 2007. Practical Heavy Oil Recovery.

Ivory, J., Zheng, R., Nasr, T., Deng, X., Beaulieu, G., Heck, G., 2008. Investigation of Low Pressure ES-SAGD. Paper SPE 117759 Presented at 2008 SPE International Thermal Operations and Heavy Oil Symposium, Calgary, Alberta, Canada, October 20–23.

Jha, R.K., Kumar, M., Benson, I., Hanzlik, E., 2013. New insights into steam/solvent-coinjection-process mechanism. SPE J. 18 (5), 867–877.

Jiang, Q., Butler, R.M., 1996. Experimental studies on effects of reservoir heterogeneity on the VAPEX process. J. Can. Pet. Technol. 35 (10), 46–54.

Johnson, S.E., 1985. Gas-Free and Gas-Saturated Bitumen Viscosity Prediction Using the Extended Principe of Corresponding States (M.Sc. thesis). University of Calgary, Calgary, Alberta.

Keshavarz, M., Okuno, R., Babadagli, T., 2013a. Optimal application conditions for steam–solvent coinjection. SPE REE (Submitted for publication).

Keshavarz, M., Okuno, R., Babadagli, T., 2013b. A semi-analytical solution to optimize single-component solvent coinjection with steam. SPE J. (Submitted for publication).

Kisman, K.E., Yeung, K.C., 1995. Numerical Study of the SAGD Process in the Burnt Lake Oil Sands Lease. SPE International Heavy Oil Symposium, Calgary, Alberta, Canada, June 19–21.

Kumar, A., Okuno, R., 2013. Characterization of reservoir fluids using an EOS based on perturbation from n-alkanes. Fluid Ph. Equilib. 358, 250–271.

Le Ravalec, M., Morlot, C., Marmier, R., Foulon, D., 2009. Heterogeneity impact on SAGD performance in mobile heavy oil reservoirs. Oil Gas Sci. Technol. – Rev. IFP 64 (4), 469–476.

Leaute, R.P., 2002. Liquid Addition to Steam for Enhancing Recovery of Bitumen with CSS: Evolution of Technology from Research Concept to a Field Pilot at Cold Lake. SPE/Petroleum Society of CIM/CHOA Paper Number 79011, Calgary, Alberta, Canada, November 4–7.

Leaute, R.P., Carey, B.S., 2005. Liquid Addition to Steam for Enhancing Recovery (LASER) of Bitumen with CSS: Results from the First Pilot Cycle. Paper Number 2005-161 Presented at the 56th Canadian International Petroleum Conference, Calgary, Alberta, Canada, June 7–9.

Leontaritis, K.J., Mansoori, G.A., 1987. Asphaltene Flocculation During Oil Production and Processing: A Thermodynamic Cloidal Model. Paper SPE 16258 Presented at the SPE International Symposium on Oilfield Chemistry, San Antonio, Texas. February 4–6.

Li, W., Mamora, D.D., 2010. Phase Behavior of Steam with Solvent Coinjection under Steam Assisted Gravity Drainage (SAGD) Process. Paper SPE 130807 Presented at the SPE EUROPEC/EAGE Annual Conference and Exhibition, Barcelona, Spain, June 14–17.

Li, W., Mamora, D.D., Li, Y., 2011a. Light-and heavy-solvent impacts on solvent-aided-SAGD process: a low-pressure experimental study. J. Can. Pet. Technol. 50 (4), 19–30.

Li, W., Mamora, D.D., Li, Y., 2011b. Solvent-type and -ratio impacts on solvent-aided SAGD process. SPE REE 14 (3), 320–331.

Mehrotra, A.K., Svrcek, W.Y., 1986. Viscosity of compressed Athabasca bitumen. Can. J. Chem. Eng. 64 (5), 844–847.

Mehrotra, A.K., Svrcek, W.Y., 1987. Corresponding states method for calculating bitumen viscosity. J. Can. Pet. Technol. 26 (5), 60–66.

Mohammadzadeh, O., Rezaei, N., Chatzis, I., 2010. Pore-Level Investigation of Heavy Oil and Bitumen Recovery Using Hybrid SAGD Process. Paper SPE 130011 Presented at the SPE Improved Oil Recovery Symposium, Tulsa, Oklahoma, USA, April 24–28.

Mokrys, I.J., Butler, R.M., 1993. In-Situ Upgrading of Heavy Oils and Bitumen by Propane Deasphalting: The Vapex Process. Paper SPE 25452 Presented at the Production Operation Symposium, Oklahoma City, 21–23 March.

Nakornthab, K., Evans, R.D., 1986. Temperature-dependent relative permeabilities and its effects on oil displacement by thermal methods. SPERE May, 230–242.

Nasr, T.N., Ayodele, O.R., 2006. New Hybrid Steam–Solvent Processes for the Recovery of Heavy Oil and Bitumen. Paper SPE 101717 Presented at Abu Dhabi International Petroleum Exhibition and Conference, Abu Dhabi, U.A.E., November 5–8.

Nasr, T.N., Beaulieu, G., Golbeck, H., Heck, G., 2003. Novel expanding solvent-SAGD process "ES-SAGD". J. Can. Pet. Technol. 42 (1), 13–16.

Nasr, T., Isaacs, E., 2001. Process for Enhancing Hydrocarbon Mobility Using a Steam Additive. U.S. Patent 6230814.

Nghiem, L.X., Sammon, P.H., Kohse, B.F., 2001. Modeling Asphaltene Precipitation and Dispersive Mixing in the Vapex Process. Paper SPE 66361 Presented at the SPE Reservoir Simulation Symposium, Houston, Texas, February 11–14.

Peng, D.-Y., Robinson, D.B., 1976. A new two-constant equation of state. Ind. Eng. Chem. Fundum. 15 (1), 59–64.

Polikar, M., Farouq Ali, S.M., Puttagunta, V.R., 1990. High temperature relative permeabilities for Athabasca oil sands. SPE Reserv. Eng. February, 25–32.

Redford, D.A., Luhning, R.W., 1999. In situ recovery from the Athabasca oil sands-past experience and future potential, Part II. J. Can. Pet. Technol. 38 (13), 1–13.

Rachford Jr., H.H., Rice, J.D., 1952. Procedure for use of electronic digital computers in calculating flash vaporization hydrocarbon equilibrium. Pet. Trans., AIME 195, 327–328.

Sarkar, M., 1984. Property Prediction of Gas Saturated Bitumen (M.Sc. thesis). University of Calgary, Calgary, Alberta, Canada.

Sharma, J., Gates, I.D., 2010. Multiphase flow at the edge of a steam chamber. Can. J. Chem. Eng. 88 (3), 312–321.

Suranto, Bae, W., Widyaningsih, R., Muslim, M., Gunadi, T.A., Permadi, A.K., 2013. Managing of Hybrid Steam–Solvent Injection Distribution for Maximizing Recovery Factor in Heterogeneous Reservoir. Paper SPE 167367 Presented at the SPE Kuwait Oil and Gas Show and Conference, Mishref, Kuwait, October 7–10.

Yazdani, A., Alvestad, J., Kjonsvik, D., Gilje, E., Kowalewski, E., 2011. A Parametric Simulation Study for Solvent Co-Injection Process in Bitumen Deposits. Paper SPE 148804 Presented at the Canadian Unconventional Resources Conference, Calgary, Alberta, Canada, November 15–17.